



Article

PM Dimensional Characterization in an Urban Mediterranean Area: Case Studies on the Separation between Fine and Coarse Atmospheric Aerosol

Maurizio Manigrasso ^{1,*}, Maria Eleonora Soggiu ² , Gaetano Settimo ² , Marco Inglessis ², Carmela Protano ³ , Matteo Vitali ³  and Pasquale Avino ^{4,*} 

¹ Department of Technological Innovations, INAIL, Via IV Novembre 144, 00187 Rome, Italy

² Department of Environment and Health, Italian National Institute of Health, 299 Viale Regina Elena, 00161 Rome, Italy; mariaeleonora.soggiu@iss.it (M.E.S.); gaetano.settimo@iss.it (G.S.); marco.inglessis@iss.it (M.I.)

³ Department of Public Health and Infectious Diseases, Sapienza University of Rome, Piazzale Aldo Moro, 5, 00185 Rome, Italy; carmela.protano@uniroma1.it (C.P.); matteo.vitali@uniroma1.it (M.V.)

⁴ Department of Agricultural, Environmental and Food Sciences (DiAAA), University of Molise, Via F. De Sanctis, 86100 Campobasso, Italy

* Correspondence: m.manigrasso@inail.it (M.M.); avino@unimol.it (P.A.)

Abstract: Fine particulate matter (PM) is object of particular attention due to its health effects. It is currently regulated by adopting PM_{2.5} as an indicator to control anthropogenic combustion emissions. Therefore, it is crucial to collect aerosol samples representative of such sources, without including PM from natural sources. Thus, a clean separation between coarse and fine mode aerosol should be set. With this purpose, aerosol size mass distribution was taken in the aerodynamic diameter range from 0.5 to 10 µm. In comparison with a base scenario, characterized by local pollution sources, three case studies were considered, involving desert dust advection, sea salt advection and forest fire aerosol from a remote area. In the base scenario, PM_{2.5} represented a suitable fine-mode indicator, whereas it was considerably affected by coarse PM in case of desert dust and sea salt aerosol advection. Such interference was considerably reduced by setting the fine/coarse separation at 1.0 µm. Such separation underrepresented fine PM from forest fire long-range transport, nonetheless in the case studies considered, PM₁ represented the best indicator of fine aerosol since less affected by coarse natural sources. The data presented clearly support the results from other studies associating the health effects of PM_{2.5} to PM₁, rather than to PM_{1–2.5}. Overall, there is a need to reconsider PM_{2.5} as an indicator of fine atmospheric aerosol.

Keywords: PM_{2.5}; PM₁; fine aerosol; coarse aerosol; anthropogenic sources; natural sources



Citation: Manigrasso, M.; Soggiu, M.E.; Settimo, G.; Inglessis, M.; Protano, C.; Vitali, M.; Avino, P. PM Dimensional Characterization in an Urban Mediterranean Area: Case Studies on the Separation between Fine and Coarse Atmospheric Aerosol. *Atmosphere* **2022**, *13*, 227. <https://doi.org/10.3390/atmos13020227>

Academic Editor:
Liudmila Golobokova

Received: 29 December 2021

Accepted: 27 January 2022

Published: 29 January 2022

Publisher's Note: MDPI stays neutral with regard to jurisdictional claims in published maps and institutional affiliations.



Copyright: © 2022 by the authors. Licensee MDPI, Basel, Switzerland. This article is an open access article distributed under the terms and conditions of the Creative Commons Attribution (CC BY) license (<https://creativecommons.org/licenses/by/4.0/>).

1. Introduction

Particulate matter (PM) atmospheric pollution started becoming a serious health problem at the beginning of the 19th century, when steadily increasing industrialization caused the release into the atmosphere of growing amounts of pollutants. Nonetheless, it was in 1987 that PM₁₀ limits were set for the first time by the United States Environmental Protection Agency (USEPA) (52 FR 24634) and in 1999 by the European Union (EU) [1]. Therefore, epidemiological associations with the health effects observed have been established with the available PM₁₀ data. Human exposure to high PM₁₀ levels has been associated to different adverse health effects involving the cardiovascular and respiratory systems, especially in subjects with pre-existing diseases; besides, PM₁₀ exposure can be determine lung cancer, and various kind of allergies [2–5]. Finally, in 2013, more than 1000 studies and pieces of scientific evidence led the International Agency for Carcinogenic Research (IARC) to define outdoor air pollution, with particular attention to particulate matter, as carcinogenic to humans [6].

Prompted by the observation of severe adverse health effects, after short- and long-term exposure, and occurring even if in pollution conditions are in compliance with the PM₁₀ standards, the US EPA promulgated on the 1997 NAAQS for PM_{2.5}, adopting PM_{2.5} as the indicator for fine particles and identifying PM_{2.5–10} as the coarse fraction of atmospheric aerosol [7]. PM_{2.5} was regulated by the EU in 2008 by the directive 2008/50/EC [8]. Relying on the availability of PM_{2.5} databases, stronger associations between aerosol pollution and mortality have emerged when PM_{2.5} has been considered instead of PM₁₀ [9–11]. PM_{2.5} has been recognized as one of the main environmental risk factors, contributing to several adverse negative outcomes for human health impacts such as cerebrovascular diseases, chronic obstructive pulmonary disease, lung cancer, lower respiratory infections among the young and premature mortality cases [12–16].

World Health Organization (WHO) points out that scientific knowledge of the role of PM in its finer dimensions for health effects, for short- and long-term exposures, is also growing. Indeed, the ever-increasing scientific evidence on the relationship between PM₁₀ or PM_{2.5} exposure and a broad range of diseases affecting cardiovascular, respiratory, neurological and other organ systems has recently led the WHO to lower the PM Air Quality Guidelines (AQG) as well as for other pollutants such as CO, NO₂, SO₂, and O₃. With respect to the annual mean values, they have been reduced from 25 to 15 $\mu\text{g m}^{-3}$ for PM₁₀ and from 10 to 5 $\mu\text{g m}^{-3}$ for PM_{2.5}. In addition, the daily average values have been decreased from 50 to 45 $\mu\text{g m}^{-3}$ for PM₁₀ and from 20 to 15 $\mu\text{g m}^{-3}$ for PM_{2.5} [17].

More recently, many studies have focused their attention on a smaller size fraction, below 1 μm (PM₁). Chen et al. [18] found positive associations between short-term exposure to PM and circulating biomarkers of inflammation, coagulation, and vasoconstriction. Such associations were strongest for the 0.25–0.40 μm size fraction and for PM₁, when particle concentrations were expressed on number and mass metrics, respectively. Moreover, the strongest effects were observed within the first 12–24 h post-exposure period, with acute effects reported even after 2 h. Chen et al. [19] showed that the emergency hospital visits in 26 Chinese cities were significantly associated with PM₁ and PM_{2.5} monitoring data and concluded that most of them, though attributed to PM_{2.5}, were due to PM₁. Lin et al. [20], investigating the cardiovascular mortality in Guangzhou (China), reported significant associations with PM₁₀, PM_{2.5} and PM₁, whereas no significant effect was observed for PM_{2.5–10} and PM_{1–2.5}. The author concluded that the cardiovascular effects of PM₁₀ and PM_{2.5} were possibly due to PM₁. Yin et al. [21] relying on PM₁ data from 65 Chinese cities, showed that a 10 $\mu\text{g m}^{-3}$ PM₁ increase was associated to a 0.19% increased risk in non-accidental mortality, about the same as for PM_{2.5} and to a 0.29% increased risk of cardiovascular diseases, 21% higher than observed for PM_{2.5}. Yang et al. [22] compared the associations between children's lung functions in northeast China cities with the exposure to PM. They found stronger associations for PM₁ than PM_{2.5}.

From this body of evidence, the need emerges to improve the knowledge on PM₁ and, relying on it, to develop relevant air quality standards [23,24]. Within this context, the purpose of this paper is to investigate how the aerosol sources that determine PM pollution in an urban area contribute to PM_{2.5} and PM₁ concentrations and where the cut-off point between fine anthropogenic combustion aerosol and coarse aerosol from natural sources could be properly set. This task is highly relevant from a health point of view because, depending on the relevant sources, aerosol size and chemical composition change and, accordingly, the site of deposition into the respiratory system and the biological response as well change. Therefore, improving the accuracy of discrimination of aerosol from natural and anthropogenic sources into proper PM_x conventions would enhance the strength of the statistical associations between the relevant aerosol concentrations and the health effects observed. To this purpose, we have considered a basic scenario (February 2012), where aerosol pollution was determined by local sources (anthropogenic combustion sources and resuspension of aerosol from crustal origin) and three other scenarios characterized by the additional contribution of aerosol from remote areas: (i) desert dust advection (January 2013), (ii) sea salt aerosol advection, (April 2009) (iii) forest fire burning (April 2020).

2. Materials and Methods

Aerosol measures carried out at the INAIL's building in downtown Rome (41°53'46" N, 12°29'46" E) were used for the analysis of the basic, desert dust and sea salt aerosol advection scenarios, whereas those acquired at the Italian National Institute of Health (ISS)'s building (41°54'16" N, 12°31'02" E) were used for the forest fire burning scenario. Aerosol size number distributions were measured in the aerodynamic diameter (d_a) range of 0.5 μm –10 μm , by means of an Aerodynamic Particle Sizer (mod. 3321 APS, TSI, Shoreview, MN, USA). The instrument relies on the correlation of the lag of a particle behind a carrier gas in an accelerating flow field with its aerodynamic diameter [25,26]. It measures the time of flight of each sampled particle, once it is accelerated through a nozzle, by means of two overlapping laser beams. Particles are counted and sized in fifty size channels, in the range 0.5–20 μm . Measurements were taken with 5 min and 1 h time resolution at the INAIL and ISS buildings, respectively. Aerosol size mass distribution have been calculated supposing spherical particles with 1.5 g cm^{-3} density [27–29]. The dynamic properties of the Planetary Boundary Layer (PBL) were estimated by means of a PBL Mixing Monitor (FAI Instruments, Fonte Nuova, Italy) at 1 h time resolution [30]. The instrument samples atmospheric PM on 47-mm membrane filters, where a Geiger detector measures the β -radioactivity of short-lived decay products of Radon (^{222}Rn). For the sea salt advection scenario, the ionic fraction of $\text{PM}_{2.5}$ has been measured by means of an URG-9000 ambient ion monitor (Chapel Hill, NC, USA) equipped with two ion chromatograph, which allows direct measurements with hourly time resolutions of cations and anions [31]. For the desert dust advection scenario, the PM_{10} chemical analysis were obtained from the data of Institute of Atmospheric Pollution Research (IIA), National Research Council (CNR) in Montelibretti (about 30 km north-east from Rome), made available in the framework of the European Monitoring and Evaluation Programme (EMEP) (data available at <http://ebas.nilu.no/> (last access on 18 December 2021)).

3. Results

3.1. Basic Scenario—Local Pollution Sources

Atmospheric aerosols, based on their origin and on their particle size, are currently described by two main fractions: a coarse one, identified as PM_{10} – $\text{PM}_{2.5}$ and a fine one, identified as $\text{PM}_{2.5}$, which includes ultrafine ($d_a < 0.1 \mu\text{m}$) and accumulation mode particles (0.1–1 μm). Fine mode aerosol derives mainly from primary anthropogenic combustion sources and from secondary processes, whereas coarse mode PM derives from soil and road dust resuspension [32–34], and from natural sources, such as desert dust [35,36] and sea salt aerosol [37,38]. The two modes, given that their emission sources are completely different, are independent one from the other. Due to the well-known effects of exposure to air pollution and PM on human health, it is crucial to work on both reducing emissions and regulating and controlling ambient concentrations of $\text{PM}_{2.5}$ as the indicator for fine.

In downtown Rome, in winter period, on average, PM_{10} is made of primary anthropogenic aerosol (31%), secondary aerosol (36%), crustal material (25%) and sea salt aerosol (8%) [39]. Figure 1 describes the aerosol mass size distributions peculiarly measured in downtown Rome, during the rush hours in wintertime, in pollution conditions mainly determined by local sources. In such conditions, the cut-off point between fine and coarse mode can be set in between 1.0 μm and 1.5 μm . Nonetheless, a 2.5 μm cut-off point represents a suitable separation between the two fractions, since it includes only a small portion of the lower tail of the coarse size mass distribution.

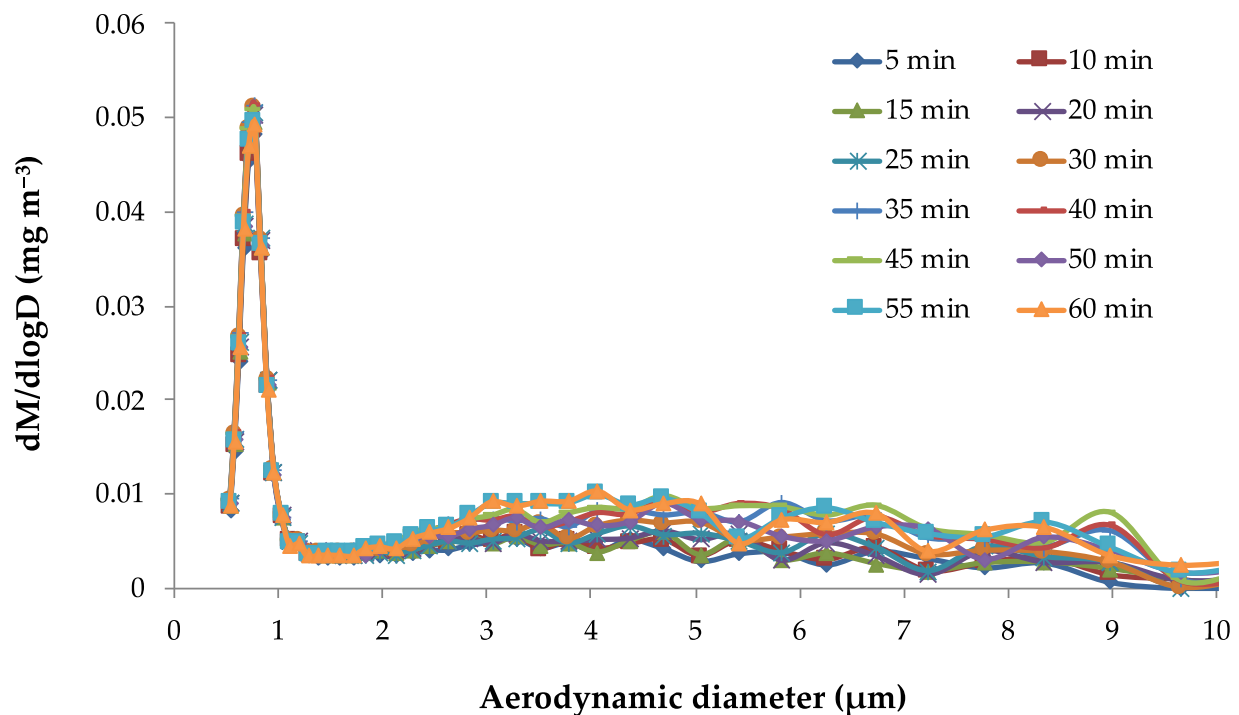


Figure 1. 5 min-time resolution aerosol size mass distribution in downtown Rome, during rush-hour (7 February 2012, 7–8 a.m.) in wintertime.

3.2. Desert Dust Advection—Transition from a Mainly Fine to a Mainly Coarse Mode Aerosol

Dust from desert areas can be uplifted at high altitude into the atmosphere and be transported over long distances on a synoptic scale [40,41]. Saharan dust advection represents a source of coarse aerosol in the Mediterranean basin [42,43]. Saharan dust was transported over Rome on 30% of the days of 2001, causing an average contribution to PM_{10} concentrations of about $15.6 \mu g m^{-3}$ [36]. Worldwide, Kok et al. [44] estimated that a 22–29 Tg global loading of dust derives 50% from North African regions, 40% from Asian regions and 10% from North American and Southern Hemisphere regions.

Surface aerosol concentrations at the receptor sites become affected when the PBL mixing height increases to the extent that it intercepts the dust laden air mass. Peculiarly, due to the increased atmospheric dilution, this occurrence causes the reduction of the concentrations of ground emitted pollutants, whereas the surface concentration of pollutants transported at high altitude increases [41,45]. In Figure 2a the temporal trends of aerosol mass concentrations measured by APS are reported for some size channels in the range $0.5\text{--}3.5 \mu m$. Figure 2b,c show for the same time interval the temporal trends of the natural radioactivity associated to short lived decay products of radon and of CO and NO. The measurement of natural radioactivity represents a useful tool to infer information on the dynamic evolution of the PBL mixing height. Furthermore, ^{222}Rn is a natural occurring radioactive gas from soil ground emitted gas, and for a given geographical region its emission rate is constant in the regional scale of some kilometers [46,47]; it does not undergo any chemical transformation. Therefore, ^{222}Rn and its short-lived decay products concentrations merely depend on the degree of atmospheric dilution, namely on PBL mixing height and on the presence of advective conditions [48,49]. On 20 January 2013 natural radioactivity sharply decreased (Figure 2b); concurrently, the concentrations of CO and NO, primary pollutants associated to local combustion sources, also decreased (Figure 2c).

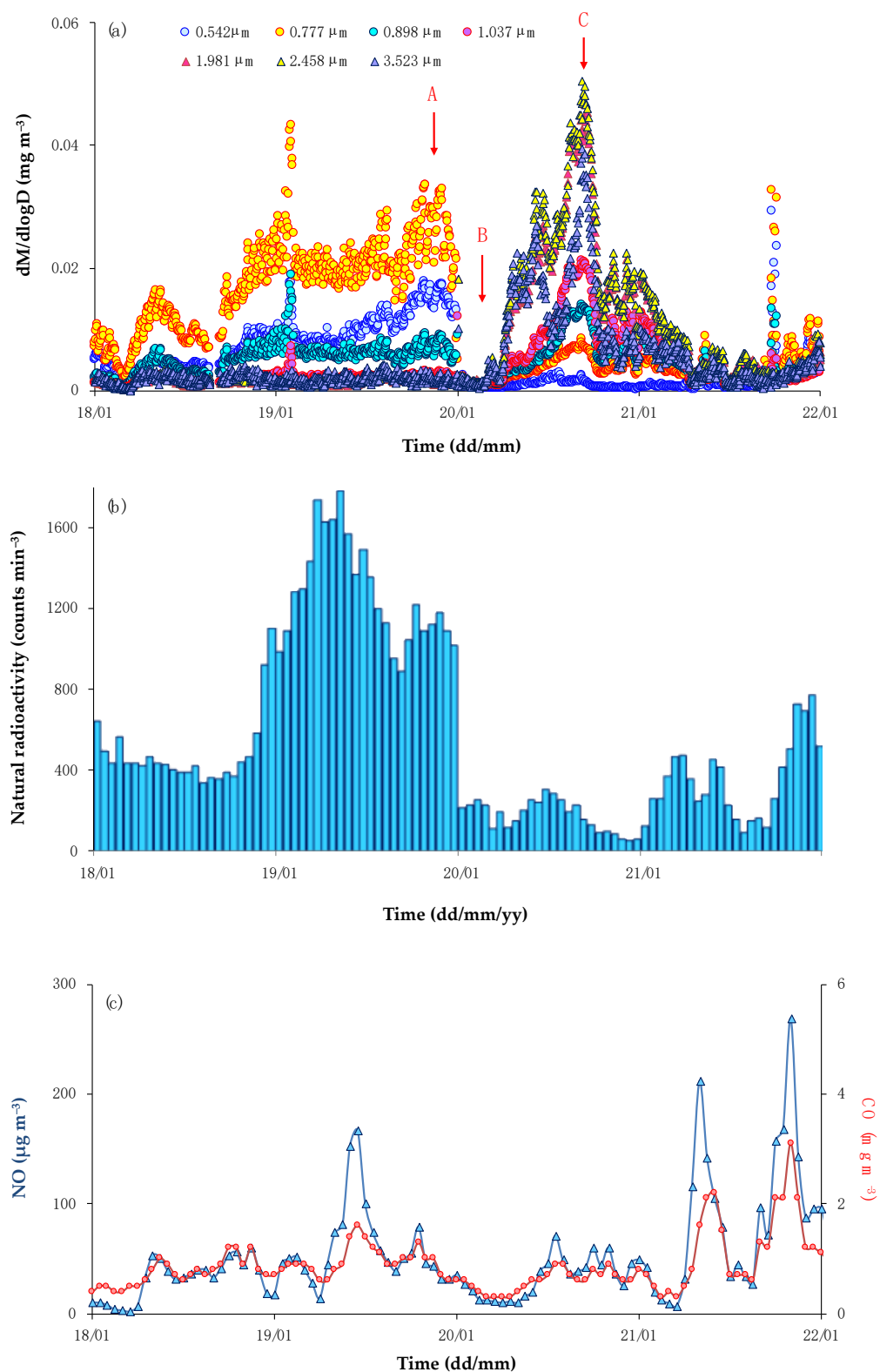


Figure 2. Temporal trends in downtown Rome (18–21 January 2013) of the APS aerosol mass concentrations for some size channels in the range 0.5–3.5 μm (a), natural radioactivity associated to short lived decay products of ^{222}Rn (b), CO and NO (c).

As a result of the increased dilution, the 0.5 μm particle concentration also abruptly decreased (Figure 2a). Conversely, the concentration of particles with sizes above 1 μm steeply increased. Such behavior can be explained by the entrainment into the PBL mixing

height of an aerosol source present in a higher atmospheric layer. Indeed, the dust forecasts carried out by the Dust REgional Atmospheric Model (DREAM) developed by the Earth Sciences Division of the Barcelona Supercomputing Center (BSC) (Figure S1) [49,50], and the NOAA HYSPLIT backward trajectories (Figure S2) [51,52], show the advection over Rome on 20 January 2013 of dust from north-western Saharan desert reaching the ground. PM₁₀ chemical analysis data carried out by IIA-C.N.R. at the EMEP monitoring site (data available at <http://ebas.nilu.no/>, last access on 18 December 2021) conclusively confirms such an interpretation (Figure 3).

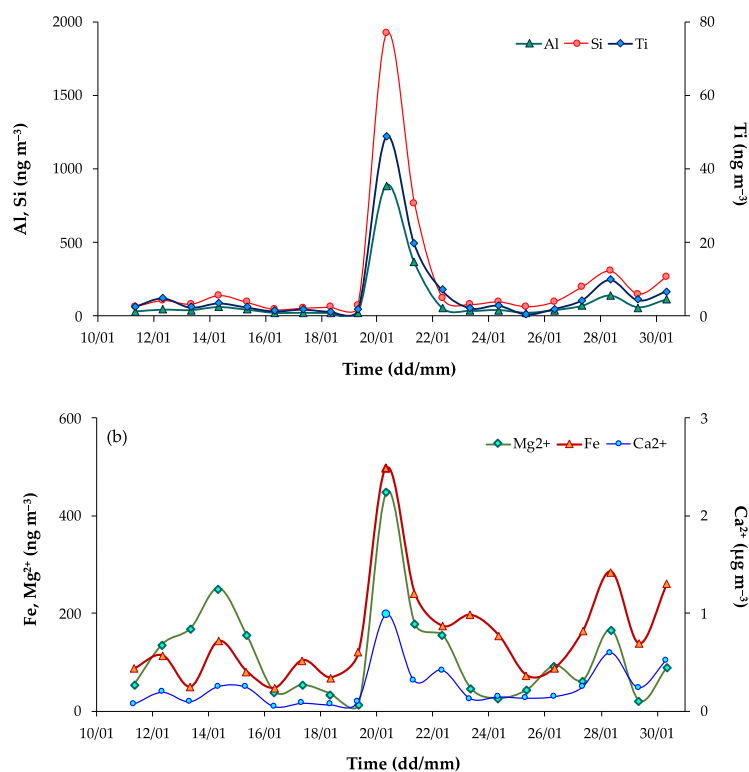


Figure 3. Daily concentrations trends of Al, Si, Ti in PM₁₀ concentrations (a), and Mg²⁺, Fe, Ca²⁺ in PM₁₀ concentrations (b) measured by IIA-CNR at the EMEP monitoring site in Montelibretti (Rome) from 10 to 30 January 2013.

On 20 January 2013 the daily concentration trends of mineral dust markers such as aluminum, silicon and titanium [53,54] exhibited peak values (Figure 3a). Specifically, in agreement with HYSPLIT back-trajectories (Figure S2), on 20 January 2013 the Al/Si ratio was 2.17, concurrent with the range between 1 and 7 reported for northern African and eastern Asian dust samples [55,56]. Moreover, the elemental (Ca + Mg)/Fe ratio of 2.89 was also in agreement with the dust provenience from northern Africa. Such a ratio has been reported to be greater than 1 for dust coming from Atlas region, central Algeria, Libya, and Egypt and lower than 1 for the sub-Saharan region [54,56].

Figure 4 shows the temporal evolution of the aerosol size mass distributions for the 1h-time intervals highlighted with arrows in Figure 2a. Before the marked increase of the PBL mixing height (Figure 2b), aerosol pollution was dominated by the fine fraction, with a mode below 1 µm (Figure 4a). When the PBL mixing height steeply increased, the fine aerosol concentration markedly dropped, because it was associated to local sources of pollution and due to the increased atmospheric dilution (Figure 4b). Few hours later, because of the increased PBL mixing height, the Saharan dust transported at high quote reached the ground and the aerosol size mass distribution exhibited an intense broad coarse mode centered at about 2.5 µm (Figure 4c). In such conditions, the mass size distributions changed from having a maximum at below 1 µm (Figure 4a) to maximum values at about 2.5 µm (Figure 4c). Before this transition occurred the aerosol levels dramatically dropped

(Figure 4b) due to strong dilution of local sources. When desert dust reached the ground the local source contribution was very low and $PM_{2.5}$ was almost completely made of desert dust. It is worth observing that, in agreement with the findings of Gobbi et al. [40] and of Manigrasso et al. [41,45], the tail of the coarse fraction extended below $1\ \mu m$, as also shown by the $0.77\ \mu m$ and $0.89\ \mu m$ size fractions that, even if at markedly lower concentrations, shared the same temporal trend of the size fractions above $>1\ \mu m$ (Figure 2a).

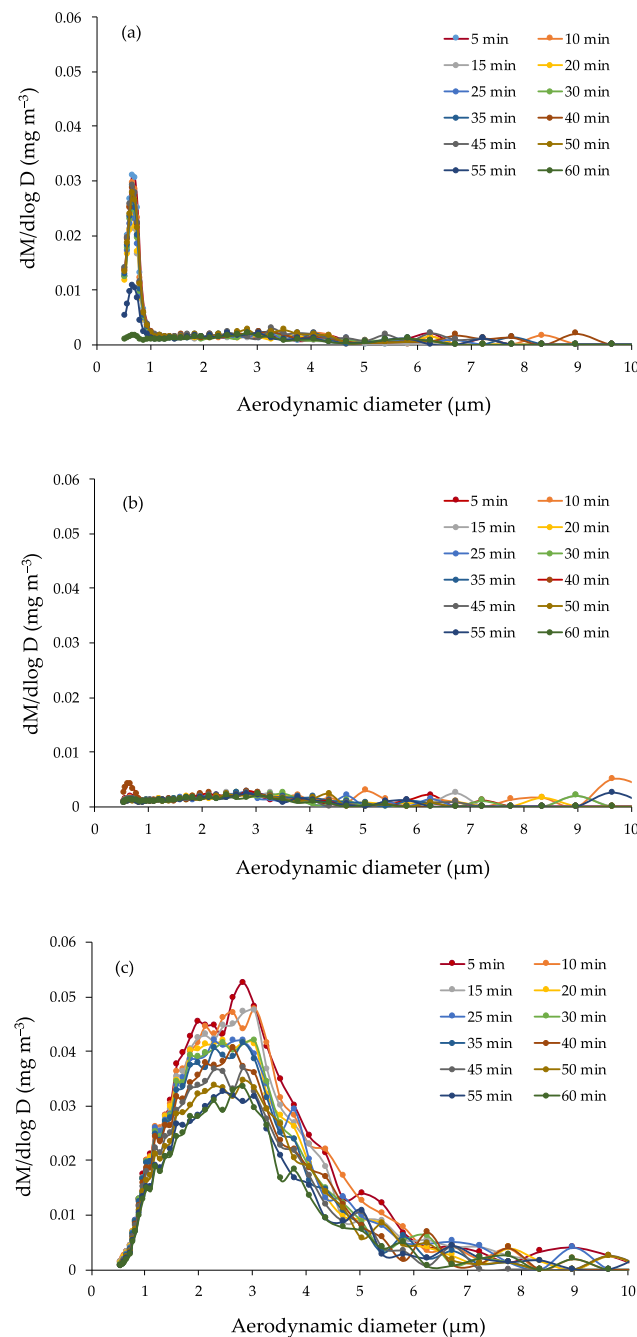


Figure 4. The 5 min-time resolution aerosol size mass distributions for the 1 h-time intervals highlighted with arrows in Figure 2a.

3.3. A Coarse Aerosol Period—Desert Dust Followed by Sea Salt Aerosol Advection

Desert dust advection occurred over Rome on 27 April 2009, as shown by the DREAM dust loading (Figure S3) and by the NOAA Hysplit backward trajectories (Figure S4). As previously discussed, the size fractions from $0.78\ \mu m$ to $3.5\ \mu m$ (Figure 5a) reached peak

concentrations when the level of natural radioactivity dropped, due to the increased PBL mixing height (Figure 5b). Coherently, in the same period, such size fractions followed the same temporal trend of Ca^{2+} ions measured on $\text{PM}_{2.5}$ fraction (Figure 5c) because of the strong desert dust contribution. At the end of 27, on 28 and on 29–30 April 2009 the size fractions from about $0.8 \mu\text{m}$ to $3.5 \mu\text{m}$ ceased to follow the Ca^{2+} temporal trend and followed the trends of Na^+ and Cl^- ions, suggesting the advection of sea salt aerosol. Coherently, the wind direction in the same periods changed from an offshore to an onshore direction (Figure S5).

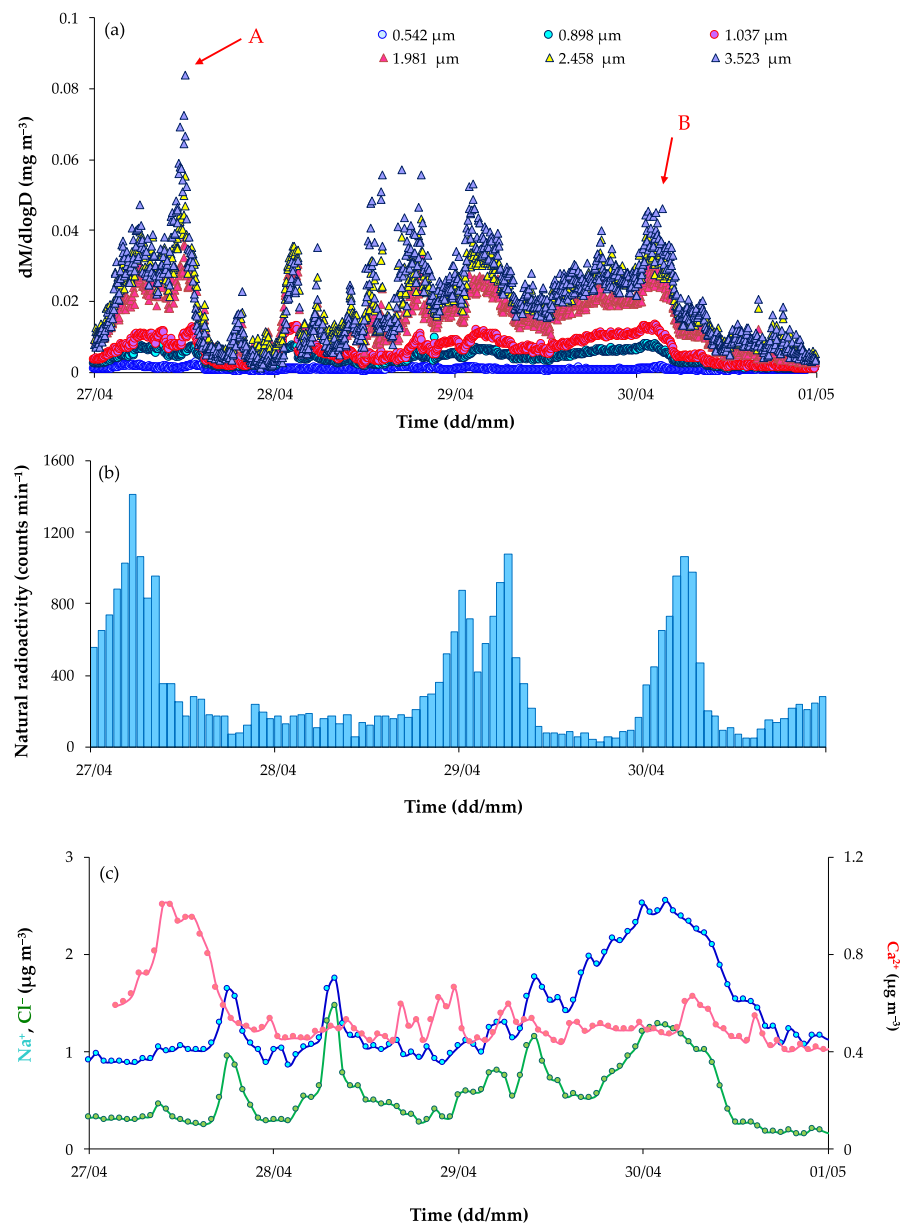


Figure 5. Temporal trends in downtown Rome (27–30 April 2009) of the APS (INAIL Building) aerosol mass concentrations for some size channels in the range $0.5\text{--}3.5 \mu\text{m}$ (a), natural radioactivity associated to short lived decay products of ^{222}Rn (b), $\text{PM}_{2.5}$ Na^+ , Cl^- and Ca^{2+} concentrations (c).

The size mass distribution characterizing the two periods of desert dust (a) and of sea salt aerosol advection (b) are reported in Figure 6. In both cases, a broad coarse mode was observed, centered at about $4 \mu\text{m}$, with a strong contribution at $2.5 \mu\text{m}$ and a lower tail extending below $1.0 \mu\text{m}$.

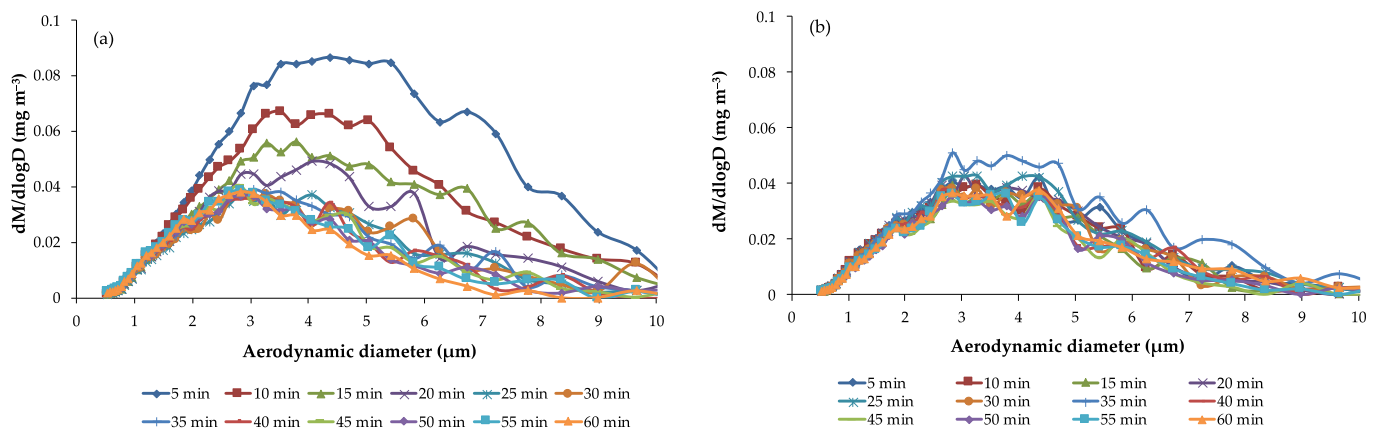


Figure 6. 5 min time-resolution aerosol size mass distributions characterizing two periods of desert dust (a) and of sea salt aerosol advection (b) for the 1 h-time intervals highlighted with arrows in Figure 5a.

3.4. Forest Fires

Drought and high temperature weather conditions, more and more frequent due to the global climate change, have been causing the worldwide alarming increase of the frequency and of the extension of forest fires [57,58]. As a result of that, huge amounts of aerosol are released into the atmosphere and are transported over long distances.

In 2019 Ager et al. [59] expressed a growing concern over the fires ignited in the Chernobyl contaminated areas, with the risk of significant ^{137}Cs resuspension. In particular, they estimated that the risk of large wildfire was highest in the Ukrainian Chernobyl Exclusion Zone. At the beginning of April 2020 fires broke out in the Chernobyl Exclusion Zone [60–62] and the smoke plume completely invested the Italian peninsula (<https://www.youtube.com/watch?v=drBEy4V0j3I>, last access on 18 January 2022; IRSN, 2020) [63], as also shown by the NAAPS smoke surface concentration map (Figure S6).

Figure 7 shows the daily trends of the 1h- average mass concentrations of the APS (ISS Building) aerosol fractions with d_a in the size range from $0.5\ \mu\text{m}$ to $3.5\ \mu\text{m}$. These data show an intense peak of the fractions in between $0.7\ \mu\text{m}$ and $1\ \mu\text{m}$ on 9 April 2020 and a less intense one on 13 April 2020.

The NOAA HYSPLIT back trajectories at 500 m height over Rome on 9 April (Figure S7) are coherent with the transport over Rome of an air mass coming from Ukraine.

The hourly average aerosol mass size distribution before (8 April) and after (10 April), the first intense fine episode (Figure 8a,c), show that the separation between the coarse and the fine fraction can be set in between $1.0\ \mu\text{m}$ and $1.5\ \mu\text{m}$. However, the mass size distributions measured on the peak days (Figure 8b,d) are somewhat different, the fine mode is broader and its upper tail spans slightly over $1.5\ \mu\text{m}$, overlapping to some extent with the lower tail of the coarse mode. Indeed, particles of $1\text{--}2\ \mu\text{m}$ in diameter were detected in forest fire plumes at high altitude (above 10 km) by Dahlkötter et al. [64]. Moreover, the mode of the mass size distributions observed at $0.8\text{--}0.9\ \mu\text{m}$ agrees with the findings of Sapkota et al. [65] who assessed the impact of Quebec Forest fires on the air quality in Baltimore and reported particle mass size distributions below $2.5\ \mu\text{m}$ and peak PM concentration in the $0.8\text{--}0.9\ \mu\text{m}$ size range. Therefore, on 9 (Figure 8b) and 13 April (Figure 8d) the coarse-fine separation would be properly set at an aerodynamic diameter of about $1.5\ \mu\text{m}$. In any case, a $2.5\ \mu\text{m}$ cut-off point would include a portion of the coarse mode aerosol.

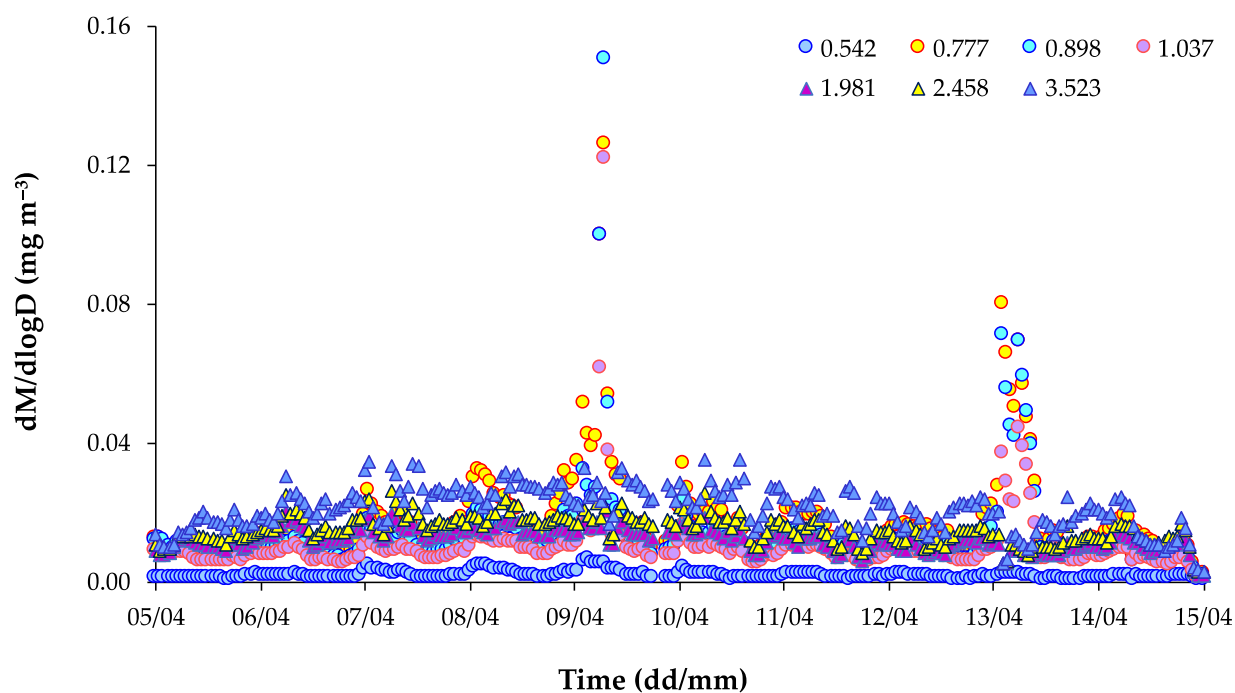


Figure 7. Temporal trends in downtown Rome of the APS aerosol mass concentrations for some size channels in the range 0.5–3.5 μm from 5 to 15 of April 2020.

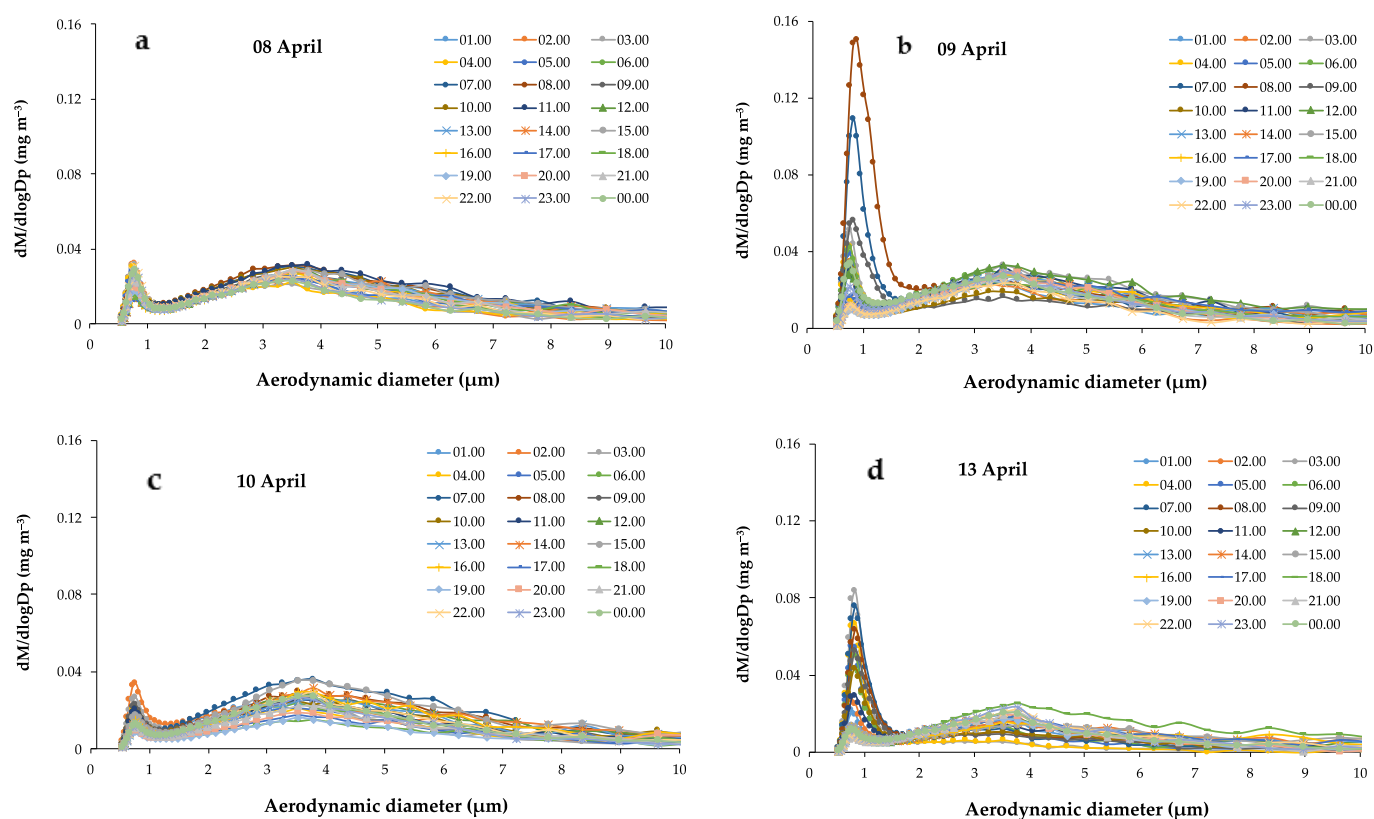


Figure 8. 1 h-time resolution Aerosol size mass distributions on 08 (a), 09 (b), 10 (c), 13 (d) April 2020 in downtown Rome.

4. Conclusions

A clean separation of fine and coarse atmospheric aerosols is relevant for understanding the anthropogenic sources emissions and for taking important policy for the public health. The case studies reported show that, when local combustion pollution sources along with road dust and crustal material are prevalent, a clear separation between fine and coarse fractions is observed and can be set at $2.5\ \mu\text{m}$. Under these circumstances, $\text{PM}_{2.5}$ can be considered a suitable indicator of the fine PM, although slightly affected by the lower tail of the coarse distribution. For such reason, the separation between the two fractions, specifically at $1.0\ \mu\text{m}$, would be more effective. In fact, under special conditions, when desert dust and sea salt aerosol advection affect the aerosol mass distribution, $\text{PM}_{2.5}$ includes a strong contribution from these other natural sources. Thus, under these circumstances, $\text{PM}_{2.5}$ would be an ineffective indicator of anthropogenic fine aerosol. The point is to avoid to erroneously include, as a $2.5\ \mu\text{m}$ separation would, a relevant fraction of desert dust and/or of sea salt aerosol in PM samples that are meant to represent combustion aerosol. It is worth observing that, in these cases, the lower tail of the size mass distributions extends below $1.0\ \mu\text{m}$, then PM_1 as well is affected, even if to considerably minor extent than $\text{PM}_{2.5}$, by the contribution of these natural sources. Forest fires are sources of pollution that are intensifying due to the effects of global climate change. The relevant aerosols share with anthropogenic combustion aerosols components that have a great impact on human health, since they elicit carcinogenic potential and are causing agents of cardiovascular and respiratory pathology exacerbation. Therefore, they should be efficiently sampled upon collecting fine PM samples. The case study presented, concerning long-range transport from a remote area, shows that the upper tail of the fine mode, where this kind of aerosol is distributed, and the lower tail of the coarse mode are to some extent overlapped, so that a proper cut-off point between the two fractions should be placed at $1.5\ \mu\text{m}$. Setting the separation between fine and coarse PM at $1.5\ \mu\text{m}$ would allow a more efficient collection of aerosols from forest fires but would be subjected to include a still important contribution from desert dust advection.

Overall, the data discussed show that PM_1 clearly represents anthropogenic combustion sources, whereas $\text{PM}_{2.5}$ may be greatly affected by natural sources. Following the WHO air quality guidelines, addressing the importance of measuring PM below $2.5\ \mu\text{m}$, in view of the human health protection, PM_1 measurements should be included in air monitoring plans.

Supplementary Materials: The following supporting information can be downloaded at: <https://www.mdpi.com/article/10.3390/atmos13020227/s1>, Figure S1: DREAM dust loading and wind field at 3000 m height in the Mediterranean area on 20 January 2013; Figure S2: NOAA HYSPLIT 72 h backward air trajectories passing over Rome, 1000 above ground level, on 20 January 2013; Figure S3: DREAM dust loading and wind field at 3000 m height in the Mediterranean area on 26 April 2009; Figure S4: NOAA HYSPLIT 72 h backward air trajectories passing over Rome, 1000 above ground level, on 28 April 2009; Figure S5: Temporal trend of wind speed and wind direction in downtown Rome on 27 April–1 May 2009; Figure S6: NAAPS smoke surface concentration on 8 April 2020 at 18.00 UTC; Figure S7: NOAA HYSPLIT 72 h backward air trajectories passing over Rome, 1000 above ground level, on 9 April 2020.

Author Contributions: Conceptualization, M.M.; methodology, M.M.; software, M.M.; validation, C.P., M.V. and P.A.; formal analysis, M.M.; investigation, M.M., M.E.S., G.S., M.I. and P.A.; resources, M.M., M.E.S., G.S., M.I. and P.A.; data curation, M.M., M.E.S., G.S., M.I., C.P., M.V. and P.A.; writing—original draft preparation, M.M. and C.P.; writing—review and editing, M.E.S., G.S., M.V. and P.A.; supervision, M.M. All authors have read and agreed to the published version of the manuscript.

Funding: This research received no external funding.

Institutional Review Board Statement: Not applicable.

Informed Consent Statement: Not applicable.

Data Availability Statement: Data is contained within the article and supplementary material.

Acknowledgments: The authors gratefully acknowledge the Institute of Atmospheric Pollution Research (IIA) of the National Research Council (CNR) for making available the PM₁₀ chemical composition data in the framework of the European Monitoring and Evaluation Programme (EMEP), the NOAA Air Resources Laboratory (ARL) for the provision of the HYSPLIT transport and dispersion model and/or READY website (<https://www.ready.noaa.gov>) used in this publication, the Naval Research Laboratory (Monterrey, USA; <https://www.nrlmry.navy.mil/aerosol/>) and the Earth Sciences Division of the Barcelona Supercomputing Center (<https://ess.bsc.es/bsc-dust-daily-forecast>) for NAAPS maps and DREAM maps, respectively (for all sites, last access on 20 December 2021).

Conflicts of Interest: The authors declare no conflict of interest.

References

1. Council Directive 1999/30/EC of 22 April 1999 Relating to Limit Values for Sulphur Dioxide, Nitrogen Dioxide and Oxides of Nitrogen, Particulate Matter and Lead in Ambient Air. Available online: <https://eur-lex.europa.eu/legal-content/EN/TXT/PDF/?uri=CELEX:31999L0030&from=EN> (accessed on 26 October 2021).
2. Chen, J.; Hoek, G. Long-term exposure to PM and all-cause and cause-specific mortality: A systematic review and meta-analysis. *Environ. Int.* **2020**, *143*, 105974. [CrossRef] [PubMed]
3. Donaldson, K.; MacNee, W. Potential mechanisms of adverse pulmonary and cardiovascular effects of particulate air pollution (PM₁₀). *Int. J. Hyg. Environ. Health* **2001**, *203*, 411–415. [CrossRef] [PubMed]
4. Fiordelisi, A.; Piscitelli, P.; Trimarco, B.; Coscioni, E.; Iaccarino, G.; Sorriento, D. The mechanisms of air pollution and particulate matter in cardiovascular diseases. *Heart Fail. Rev.* **2017**, *22*, 337–347. [CrossRef]
5. Consonni, D.; Carugno, M.; De Matteis, S.; Nordio, F.; Randi, G.; Bazzano, M.; Caporaso, N.E.; Tucker, M.A.; Bertazzi, P.A.; Pesatori, A.C.; et al. Outdoor particulate matter (PM₁₀) exposure and lung cancer risk in the EAGLE study. *PLoS ONE* **2018**, *13*, e0203539. [CrossRef] [PubMed]
6. IARC. *Monograph on the Evaluation of Carcinogenic Risks to Humans*; IARC: Lyon, France, 2013; Volume 109.
7. USEPA. The National Ambient Air Quality Standards (NAAQS) for Particulate Matter (PM): EPA's 2006 Revisions and Associated Issues; Congressional Research Service. 2013. Available online: <https://sgp.fas.org/crs/misc/RL34762.pdf> (accessed on 26 October 2021).
8. Directive 2008/50/EC of the European Parliament and of the Council of 21 May 2008 on Ambient Air Quality and Cleaner Air for Europe. Available online: <https://eur-lex.europa.eu/legal-content/en/ALL/?uri=CELEX:32008L0050> (accessed on 26 October 2021).
9. Dockery, D.W.; Pope, C.A.; Xu, X.; Spengler, J.D.; Ware, J.H.; Fay, M.E.; Ferris, B.G., Jr.; Speizer, F.E. An association between air pollution and mortality in six U.S. cities. *N. Engl. J. Med.* **1993**, *329*, 1753–1759. [CrossRef]
10. Levy, J.I.; Hammit, J.K.; Spengler, J.D. Estimating the mortality impacts of particulate matter: What can be learned from between-study variability? *Environ. Health Perspect.* **2000**, *108*, 109–117. [CrossRef]
11. WHO. *Health Effects of Particulate Matter*; WHO Regional Office for Europe: Copenhagen, Denmark, 2013; Available online: https://www.euro.who.int/__data/assets/pdf_file/0006/189051/Health-effects-of-particulate-matter-final-Eng.pdf (accessed on 26 October 2021).
12. He, C.; Huang, G.; Liu, L.; Li, Y.; Zhai, M.; Cao, R.; Weidema, B.P.; Fantke, P. Assessment and offset of the adverse effects induced by PM_{2.5} from coal-fired power plants in China Relating the global burden of disease to life cycles. *Procedia CIRP* **2018**, *69*, 417–422.
13. Xing, Y.-F.; Xu, Y.-H.; Shi, M.-H.; Lian, Y.-X. The impact of PM_{2.5} on the human respiratory system. *J. Thorac. Dis.* **2016**, *8*, E69–E74.
14. Maji, K.J.; Dikshit, A.K.; Arora, M.; Deshpande, A. Estimating premature mortality attributable to PM_{2.5} exposure and benefit of air pollution control policies in China for 2020. *Sci. Total Environ.* **2018**, *612*, 683–693. [CrossRef]
15. Zhang, S.; Routledge, M.N. The contribution of PM_{2.5} to cardiovascular disease in China. *Environ. Sci. Pollut. Res. Int.* **2020**, *27*. [CrossRef]
16. Guo, H.; Li, W.; Wu, J. Ambient PM_{2.5} and Annual Lung Cancer Incidence: A Nationwide Study in 295 Chinese Counties. *Int. J. Environ. Res. Public Health* **2020**, *17*, 1481. [CrossRef] [PubMed]
17. WHO. *WHO Global Air Quality Guidelines: Particulate Matter (PM_{2.5} and PM₁₀), Ozone, Nitrogen Dioxide, Sulfur Dioxide and Carbon Monoxide*; WHO Regional Office for Europe: Copenhagen, Denmark, 2021; Available online: <https://apps.who.int/iris/handle/10665/345329> (accessed on 26 October 2021).
18. Chen, R.; Zhao, Z.; Sun, Q.; Lin, Z.; Zhao, A.; Wang, C.; Xia, Y.; Xu, X.; Kan, H. Size-fractionated Particulate Air Pollution and Circulating Biomarkers of Inflammation, Coagulation, and Vasoconstriction in a Panel of Young Adults. *Epidemiology* **2015**, *26*, 328–336. [CrossRef] [PubMed]
19. Chen, G.; Li, S.; Zhang, Y.; Zhang, W.; Li, D.; Wei, X.; He, Y.; Bell, M.L.; Williams, G.; Marks, G.B.; et al. Effects of ambient PM₁ air pollution on daily emergency hospital visits in China: An epidemiological study. *Lancet Planet. Health* **2017**, *1*, e221–e229. [CrossRef]

20. Lin, H.; Tao, J.; Du, Y.; Liu, T.; Qian, Z.; Tian, L.; Di, Q.; Rutherford, S.; Guo, L.; Zeng, W.; et al. Particle size and chemical constituents of ambient particulate pollution associated with cardiovascular mortality in Guangzhou, China. *Environ. Pollut.* **2016**, *208*, 758–766. [CrossRef] [PubMed]
21. Yin, P.; Guo, J.; Wang, L.; Fan, W.; Lu, F.; Guo, M.; Moreno, S.B.R.; Wang, Y.; Wang, H.; Zhou, M.; et al. Higher Risk of Cardiovascular Disease Associated with Smaller Size-Fractioned Particulate Matter. *Environ. Sci. Technol. Lett.* **2020**, *7*, 95–101. [CrossRef]
22. Yang, M.; Guo, Y.-M.; Bloom, M.S.; Dharmagee, S.C.; Morawska, L.; Heinrich, J.; Jalaludin, B.; Markevych, I.; Knibbs, L.D.; Lin, S.; et al. Is PM₁ similar to PM_{2.5}? A new insight into the association of PM₁ and PM_{2.5} with children's lung function. *Environ. Int.* **2020**, *145*, 106092. [CrossRef]
23. Kan, H. The smaller, the worse? *Lancet Planet. Health* **2017**, *1*, e210–e211. [CrossRef]
24. Avino, P.; Protano, C.; Vitali, M.; Manigrasso, M. Benchmark study on fine-mode aerosol in a big urban area and relevant doses deposited in the human respiratory tract. *Environ. Pollut.* **2016**, *216*, 530–537. [CrossRef]
25. Wilson, J.C.; Liu, B.Y.H. Aerodynamic particle size measurement by laser-doppler velocimetry. *J. Aerosol Sci.* **1980**, *11*, 139–150. [CrossRef]
26. Oskouie, A.; Wang, H.-C.; Mavliev, R.; Noll, K.E. Calculated Calibration Curves for Particle Size Determination Based on Time-of-Flight (TOF). *Aerosol Sci. Technol.* **1998**, *29*, 433–441. [CrossRef]
27. Lipponen, P.; Hänninen, O.; Sorjamaa, R.; Gherardi, M.; Gatto, M.P.; Gordiani, A.; Cecinato, A.; Romagnoli, P.; Gariazzo, C. *Aerosol Processes in PAH Infiltration and Population Exposure in Rome*; EAC: Prague, Czech Republic, 2013; Available online: [https://appspricercasientifica.inail.it/expah/documenti/Lipponen%20et%20al.2013.EAC%20Prague%20on%20EXPAH%20Slides\(v5\).pdf](https://appspricercasientifica.inail.it/expah/documenti/Lipponen%20et%20al.2013.EAC%20Prague%20on%20EXPAH%20Slides(v5).pdf) (accessed on 26 October 2021).
28. Hänninen, O.; Sorjamaa, R.; Lipponen, P.; Cyrus, J.; Lanki, T.; Pekkanen, J. Aerosol-based modelling of infiltration of ambient PM_{2.5} and evaluation against population-based measurements in homes in Helsinki, Finland. *J. Aerosol Sci.* **2013**, *66*, 111–122. [CrossRef]
29. Manigrasso, M.; Protano, C.; Vitali, M.; Avino, P. Nanoparticle Behaviour in an Urban Street Canyon at Different Heights and Implications on Indoor Respiratory Doses. *Atmosphere* **2019**, *10*, 772. [CrossRef]
30. Avino, P.; Brocco, D.; Lepore, L.; Pareti, S. Interpretation of atmospheric pollution phenomena in relationship with the vertical atmospheric remixing by means of natural radioactivity measurements (radon) of particulate matter. *Ann. Chim.* **2003**, *93*, 589–594.
31. Manigrasso, M.; Abballe, F.; Jack, R.F.; Avino, P. Time-resolved measurement of the ionic fraction of atmospheric fine particulate matter. *J. Chromatogr. Sci.* **2010**, *48*, 549–552. [CrossRef]
32. Padoan, E.; Maffia, J.; Balsari, P.; Ajmone-Marsan, F.; Dinuccio, E. Soil PM₁₀ emission potential under specific mechanical stress and particles characteristics. *Sci. Total Environ.* **2021**, *779*, 146468. [CrossRef] [PubMed]
33. Hwang, H.-M.; Fiala, M.; Park, D.; Wade, T.L. Review of pollutants in urban road dust and stormwater runoff: Part 1. Heavy metals released from vehicles. *Int. J. Urban Sci.* **2016**, *20*, 334–360. [CrossRef]
34. Gelhardt, L.; Dittmer, U.; Welker, A. Relationship of particle density and organic content in sieve fractions of road-deposited sediments from varying traffic sites based on a novel data set. *Sci. Total Environ.* **2021**, *794*, 148812. [CrossRef]
35. Querol, X.; Pey, J.; Pandolfi, M.; Alastuey, A.; Cusack, M.; Pérez, N.; Moreno, T.; Viana, M.; Mihalopoulos, N.; Kallos, G.; et al. African dust contributions to mean ambient PM₁₀ mass-levels across the Mediterranean Basin. *Atmos. Environ.* **2009**, *43*, 4266–4277. [CrossRef]
36. Gobbi, G.P.; Angelini, F.; Barnaba, F.; Costabile, F.; Baldasano, J.M.; Basart, S.; Sozzi, R.; Bolignano, A. Changes in particulate matter physical properties during Saharan advections over Rome (Italy): A four-year study, 2001–2004. *Atmos. Chem. Phys.* **2013**, *13*, 7395–7404. [CrossRef]
37. Murphy, D.M.; Froyd, K.D.; Bian, H.; Brock, C.A.; Dibb, J.E.; DiGangi, J.P.; Diskin, G.; Dollner, M.; Kupc, A.; Scheuer, E.M.; et al. The distribution of sea-salt aerosol in the global troposphere. *Atmos. Chem. Phys.* **2019**, *19*, 4093–4104. [CrossRef]
38. Grythe, H.; Ström, J.; Krejci, R.; Quinn, P.; Stohl, A. A review of sea-spray aerosol source functions using a large global set of sea salt aerosol concentration measurements. *Atmos. Chem. Phys.* **2014**, *14*, 1277–1297. [CrossRef]
39. Perrino, C.; Canepari, S.; Cardarelli, E.; Catrambone, M.; Sargolini, T. Inorganic constituents of urban air pollution in the Lazio region (Central Italy). *Environ. Monit. Assess.* **2007**, *128*, 133–151. [CrossRef] [PubMed]
40. Gobbi, G.; Barnaba, F.; Di Liberto, L.; Bolignano, A.; Lucarelli, F.; Nava, S.; Perrino, C.; Pietrodangelo, A.; Basart, S.; Costabile, F.; et al. An inclusive view of Saharan dust advections to Italy and the Central Mediterranean. *Atmos. Environ.* **2019**, *201*, 242–256. [CrossRef]
41. Manigrasso, M.; Febo, A.; Guglielmi, F.; Ciambottini, V.; Avino, P. Relevance of aerosol size spectrum analysis as support to qualitative source apportionment studies. *Environ. Pollut.* **2012**, *170*, 43–51. [CrossRef] [PubMed]
42. Mitsakou, C.; Kallos, G.; Papantoniou, N.; Spyrou, C.; Solomos, S.; Astitha, M.; Housiadas, C. Saharan dust levels in Greece and received inhalation doses. *Atmos. Chem. Phys.* **2008**, *8*, 7181–7192. [CrossRef]
43. Basart, S.; Pay, M.T.; Jorba, O.; Pérez, C.; Jiménez-Guerrero, P.; Schulz, M.; Baldasano, J.M. Aerosols in the CALIOPE air quality modelling system: Evaluation and analysis of PM levels, optical depths and chemical composition over Europe. *Atmos. Chem. Phys.* **2012**, *12*, 3363–3392. [CrossRef]

44. Kok, J.F.; Adebisi, A.A.; Albani, S.; Balkanski, Y.; Checa-Garcia, R.; Chin, M.; Colarco, P.R.; Hamilton, D.S.; Huang, Y.; Ito, A.; et al. Contribution of the world's main dust source regions to the global cycle of desert dust. *Atmos. Chem. Phys.* **2021**, *21*, 8169–8193.
45. Manigrasso, M.; Costabile, F.; Di Liberto, L.; Gobbi, G.P.; Gualtieri, M.; Zanini, G.; Avino, P. Size resolved aerosol respiratory doses in a Mediterranean urban area: From PM10 to ultrafine particles. *Environ. Int.* **2020**, *141*, 105714. [\[CrossRef\]](#)
46. Lepore, L.; Brocco, D.; Avino, P. Organic elemental carbon in the atmospheric particles. *Ann. Ist. Super. Sanita* **2003**, *39*, 365–369.
47. Gregorič, A.; Drinovec, L.; Ježek, I.; Vaupotič, J.; Lenarčič, M.; Grauf, D.; Wang, L.; Mole, M.; Stanič, S.; Močnik, G. The determination of highly time-resolved and source-separated black carbon emission rates using radon as a tracer of atmospheric dynamics. *Atmos. Chem. Phys.* **2020**, *20*, 14139–14162. [\[CrossRef\]](#)
48. Avino, P.; Manigrasso, M.; Cuomo, F. Natural radioactivity as an easy and quick parameter for describing the dynamic of the Planetary Boundary Layer. *RSC Adv.* **2015**, *5*, 57538–57549. [\[CrossRef\]](#)
49. Nickovic, S.; Kallos, G.; Papadopoulos, A.; Kakaliagou, O. A model for prediction of desert dust cycle in the atmosphere. *J. Geophys. Res.* **2001**, *106*, 18113–18129. [\[CrossRef\]](#)
50. Pérez, C.; Nickovic, S.; Baldasano, J.M.; Sicard, M.; Rocadenbosch, F.; Cachorro, V. A long Saharan dust event over the western Mediterranean: Lidar, Sun photometer observations, and regional dust modeling. *J. Geophys. Res.* **2006**, *111*, 15214. [\[CrossRef\]](#)
51. Stein, A.F.; Draxler, R.R.; Rolph, G.D.; Stunder, B.J.B.; Cohen, M.D.; Ngan, F. NOAA's HYSPLIT Atmospheric Transport and Dispersion Modeling System. *Bull. Am. Meteorol. Soc.* **2015**, *96*, 2059–2077. [\[CrossRef\]](#)
52. Rolph, G.; Stein, A.; Stunder, B. Real-time Environmental Applications and Display sYstem: READY. *Environ. Model. Softw.* **2017**, *95*, 210–228. [\[CrossRef\]](#)
53. Nicolás, J.; Chiari, M.; Crespo, J.; Orellana, I.G.; Lucarelli, F.; Nava, S.; Pastor, C.; Yubero, E. Quantification of Saharan and local dust impact in an arid Mediterranean area by the positive matrix factorization (PMF) technique. *Atmos. Environ.* **2008**, *42*, 8872–8882. [\[CrossRef\]](#)
54. Scheuven, D.; Schütz, L.; Kandler, K.; Ebert, M.; Weinbruch, S. Bulk composition of northern African dust and its source sediments—A compilation. *Earth-Sci. Rev.* **2013**, *116*, 170–194. [\[CrossRef\]](#)
55. Scheuven, D.; Kandler, K. On composition, morphology and size distribution of airborne mineral dust. In *Mineral Dust—A Key Player in the Earth System*; Knippertz, P., Stuut, J.-B., Eds.; Springer: Berlin/Heidelberg, Germany, 2014; p. 35.
56. Kandler, K.; Scheuven, D. Asian and Saharan dust from a chemical/mineralogical point of view: Differences and similarities from bulk and single particle measurements. *E3S Web Conf.* **2019**, *99*, 03001. [\[CrossRef\]](#)
57. de Rigo, D.; Libertà, G.; Houston Durrant, T.; Artés Vivancos, T.; San-Miguel-Ayanz, J. *Forest Fire Danger Extremes in Europe under Climate Change: Variability and Uncertainty*; EUR 28926 EN; Publications Office of the European Union: Luxembourg, 2017; Available online: <https://publications.jrc.ec.europa.eu/repository/handle/JRC108974> (accessed on 16 December 2021).
58. Wotton, B.M.; Nock, C.A.; Flannigan, M.D. Forest fire occurrence and climate change in Canada. *Int. J. Wildland Fire* **2010**, *19*, 253–271. [\[CrossRef\]](#)
59. Ager, A.A.; Lasko, R.; Myroniuk, V.; Zibitsev, S.; Day, M.A.; Usenia, U.; Bogomolov, V.; Kovalets, I.; Evers, C.R. The wildfire problem in areas contaminated by the Chernobyl disaster. *Sci. Total Environ.* **2019**, *696*, 133954. [\[CrossRef\]](#)
60. NASA. Fires Burn in Northern Ukraine, NASA 2020. Available online: <https://earthobservatory.nasa.gov/images/146561/fires-burn-in-northern-ukraine> (accessed on 26 October 2021).
61. NASA. Sees Fires Near Chernobyl Break Out Again NASA 2020. Available online: <https://www.nasa.gov/image-feature/goddard/2020/nasa-sees-fires-near-chernobyl-break-out-again> (accessed on 26 October 2021).
62. Note d'information Incendies en Ukraine Dans la Zone d'exclusion Autour de la Centrale Tchernobyl: Point de Situation. Available online: https://www.irsln.fr/FR/Actualites_presse/Actualites/Documents/IRSN_NI-Tchernobyl-Incendie-Zone-d-Exclusion-Ukraine_15042020.pdf (accessed on 26 October 2021).
63. Incendies à Tchernobyl: Modélisation de la Dispersion du Panache en Europe en Date du 17 Avril 2020. 15 April 2020. Available online: <https://www.youtube.com/watch?v=drBEy4V0j3IIRSN> (accessed on 26 October 2021).
64. Dahlkötter, F.; Gysel, M.; Sauer, D.; Minikin, A.; Baumann, R.; Seifert, P.; Ansmann, A.; Fromm, M.; Voigt, C.; Weinzierl, B. The Pagami Creek smoke plume after long-range transport to the upper troposphere over Europe—aerosol properties and black carbon mixing state. *Atmos. Chem. Phys.* **2014**, *14*, 6111–6137. [\[CrossRef\]](#)
65. Sapkota, A.; Symons, J.M.; Kleissl, J.; Wang, L.; Parlange, M.B.; Ondov, J.; Breyse, P.N.; Diette, G.B.; Eggleston, P.A.; Buckley, T.J. Impact of the 2002 Canadian Forest Fires on Particulate Matter Air Quality in Baltimore City. *Environ. Sci. Technol.* **2005**, *39*, 24–32. [\[CrossRef\]](#) [\[PubMed\]](#)